E	sorption ratio defined by eq 1
K_{ex}	equilibrium constant defined by eq 7, kg of sorbent/dm^3
m	content in the sorbent, mol/kg of sorbent
S	mass of the sorbent, kg
V	volume of aqueous phase, dm^3
[ ]	concentration in aqueous phase or content in the sorbent, mol/dm^3 or mol/kg of sorbent
α	separation factor defined by eq 9

Subscripts

org	organic phase
s	sorbent phase
t	total
0	initial
1, 2	metal species

Literature Cited

(1) Inoue, K.; Baba, Y.; Sakamoto, Y.; Egawa, H. *Sep. Sci. Technol.* **1987**, *22*, 1349.
(2) Kauczor, H. W.; Meyer, A. *Hydrometallurgy* **1978**, *3*, 65.
(3) Matsunaga, H.; Suzuki, T. *Nippon Kagaku Kaishi* **1988**, 659.
(4) Tavlarides, L. L.; Bae, J. H.; Lee, C. K. *Sep. Sci. Technol.* **1987**, *22*, 581.
(5) Warshawsky, A. *Ion Exchange and Solvent Extraction*; Marcel Dekker: New York, 1981; Vol. 8, p 229.
(6) Akita, S.; Takeuchi, H. *J. Chem. Eng. Jpn.* **1990**, *23*, 439.
(7) Huang, T. C.; Juang, R. S. *Ind. Eng. Chem. Fundam.* **1986**, *25*, 752.

Received for review August 27, 1991. Accepted April 28, 1992.

Vapor–Liquid Equilibrium for Chlorodifluoromethane + Dimethyl Ether from 283 to 395 K at Pressures to 5.0 MPa

Joe R. Noles[†] and John A. Zollweg*

School of Chemical Engineering, Cornell University, Ithaca, New York 14853

Vapor–liquid equilibrium conditions (p–T–x–y) of the binary mixture chlorodifluoromethane (R22) + dimethyl ether (DME) have been measured for the first time along six isotherms (three subcritical and three supercritical). The mixture forms a negative (maximum boiling) azeotrope which persists to the critical line. Direct observations were made of points on the critical line. The two lower temperature isotherms are fitted to a temperature-dependent Redlich–Kister excess Gibbs free energy model. The equal area method has been used to test the thermodynamic consistency of the two lower temperature isotherms. A brief description of the apparatus is given.

Introduction

An understanding of the vapor–liquid equilibria (VLE) of mixtures whose components have strong specific interactions (association and solvation) is important to applications such as the production of synthetic fuels (*1*), supercritical fluid extraction (*2*), and development of alternative refrigerant mixtures (*3*, *4*). A number of theories have been developed to allow calculation of the vapor–liquid equilibria of associating and solvating mixtures at high pressure (>1 MPa), but they have mostly been applied to associating systems due to the scarcity of high-pressure VLE data for solvating mixtures (*5*–*7*). The few experimental high-pressure VLE studies of solvating mixtures generally contain sparse and scattered data (*8*–*10*). This laboratory has undertaken a program to provide VLE data of solvating binary mixtures over a wide temperature and pressure range (*11*, *12*) in order to test the ability of theories being developed to describe the thermodynamics of mixtures with strong specific interactions (*5*–*7*).

The purpose of this work is to examine the pressure, p, temperature, T, liquid composition, x, and vapor composition, y, dependence of the vapor–liquid equilibria of the solvating mixture chlorodifluoromethane (R22) + dimethyl ether (DME) from room temperature to the critical region. This mixture has been used commercially as an aerosol propellant. The thermodynamic consistency of the results has been examined using a maximum likelihood method and an equal area method.

[†] Present address: Exxon Chemical Co., Baton Rouge, LA 70821-0241.

Experimental Section

A schematic diagram of the apparatus is shown in Figure 1. A detailed description of the apparatus and procedures is given elsewhere (*11*). It is a dual recirculating apparatus designed to operate isothermally from 283 to 520 K and at pressures to 40 MPa. The apparatus can be divided into three functional sections: (1) the pressure generation section, (2) the equilibrium section, and (3) the sampling section.

In the pressure generation section, the two components to be studied are distilled from individual supply cylinders into Ruska screw pumps. The screw pumps are then used to pressurize and pump the pure fluids into the equilibrium section.

The equilibrium section consists of a sapphire tube pressure cell, two magnetically driven reciprocating pumps, and two sample traps housed in an insulated thermostated oven. The equilibrium cell is made from a 3.18-cm-o.d., 1.27-cm-i.d., 10.2-cm-long sapphire tube (Union Carbide Corp.) sealed by a Bridgman unsupported area seal with a Teflon gasket (*13*). To establish equilibrium, the two magnetically driven pumps are used to circulate the vapor and liquid phases.

The oven is maintained at constant temperature using an electric ceramic heater coupled with a finned heat exchanger connected to a thermostated liquid bath (Brinkmann Model RM20). The temperature is maintained within ±0.02 K using a software implemented proportional-integral-derivative (PID) controller. A 12-in. fan is used to circulate air in the oven to minimize temperature gradients. The temperature of the equilibrium cell is measured with an accuracy of 0.002 K on IPTS-68 using a platinum resistance thermometer (Leeds and Northrup Model 8164) placed in a hole drilled concentrically in the top of one of the flange bolts of the equilibrium cell.

Data acquisition and temperature control are implemented using a general-purpose interface bus (GP-IB) system consisting

0021-9568/92/1737-0306$03.00/0

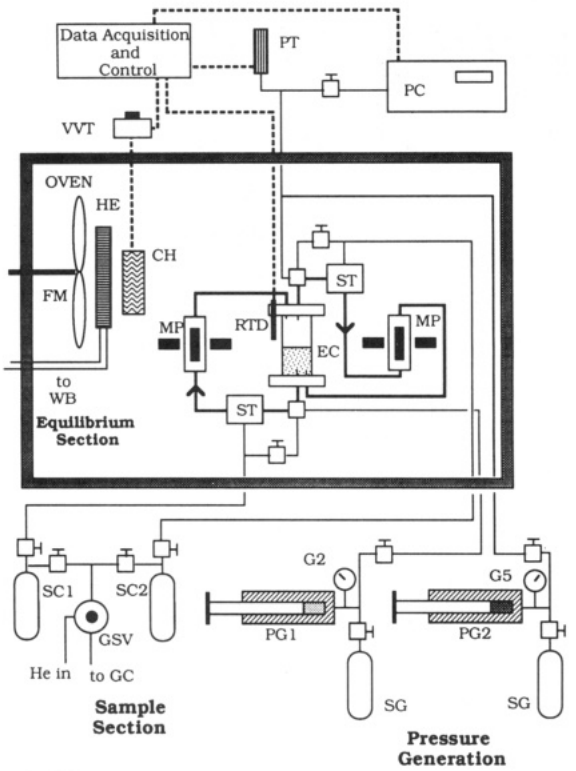

Figure 1. Schematic diagram of apparatus. Components are labeled as follows: ceramic heater (CH), equilibrium cell (EC), fan (FM), Bourdon tube gauge (G), gas sampling valve (GSV), heat exchanger (HE), magnetic pump (MP), quartz spiral pressure counter (PC), screw pump (PG), strain gage pressure transducer (PT), platinum resistance thermometer (RTD), sample collection cylinder (SC), supply cylinder (SG), liquid sample trap (SL), vapor sample trap (SV), variable voltage transformer (VVT), and refrigerated water bath (WB).

of a Macintosh SE computer, a National Instruments MacBus interface, a Hewlett-Packard 3488A switch control unit, and a Solartron 7071 computing voltmeter.

A strain gage pressure transducer (T-Hydronics Model TH-2V3) with a precision of ±0.003 MPa, as determined by numerous calibrations with a Ruska quartz spiral pressure gage (model DDR 6000) which was calibrated using a Ruska dead weight gage (model 2450), was used to measure pressure.

Two methods are available for obtaining equilibrium samples. In one method, samples are trapped without disturbing equilibrium, using a three-valve trap situated at the beginning of each circulation loop. The second method is to use capillary tubing (0.002-in. i.d.) to draw small samples directly from the equilibrium cell into the collecting cylinders. Liquid nitrogen is used to completely transfer the samples to the collecting cylinders. Sample size is such that once the collection cylinder is heated to melt and vaporize the sample, the pressure is subatmospheric (<100 kPa).

The collected samples are analyzed using a Hewlett-Packard 5890A gas chromatograph. A pneumatic sampling valve with a 0.1-mL sample volume is used to inject a sample into a 10-m Chrompack Poraplot Q 0.32-mm capillary column. A microvolume thermal conductivity detector (TCD) is used to measure the amount of each component as it passes out of the column. The output of the TCD, a dc voltage, is integrated using a Hewlett-Packard 3293A integrator whose output is a list of peak areas. Five analyses are performed on each sample to ensure that the results are reproducible.

In order to relate the area of each peak, in counts, to the amount of material, in moles, a calibration is required. Standard practice is to assume a linear relationship between peak area, A_i, and number of moles, n_i

$$n_i = k_i A_i \tag{1}$$

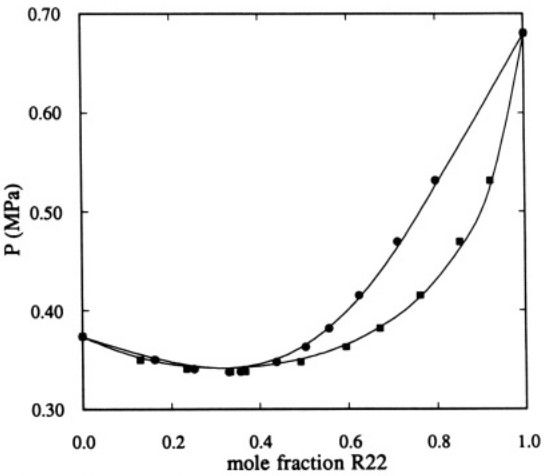

Figure 2. $p-T-x-y$ results for R22 + DME at 283.15 K. Experimental liquid compositions are denoted by ●. Experimental vapor compositions are denoted by ■. Lines are excess Gibbs free energy model prediction.

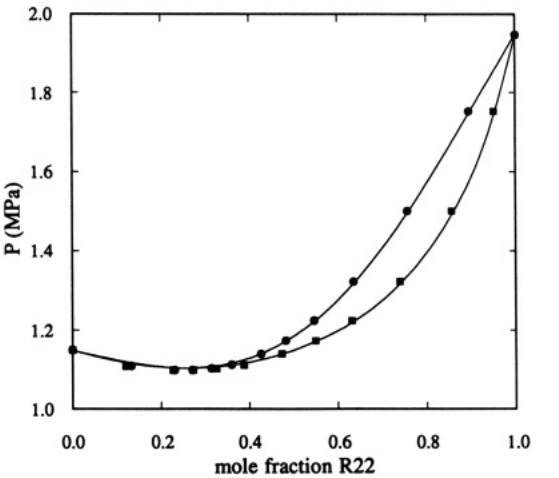

Figure 3. $p-T-x-y$ results for R22 + DME at 323.15 K. Symbols are the same as in Figure 2.

The calibration is performed by injecting pure gas samples at accurately measured subatmospheric pressures and noting the corresponding peak areas. The sample pressures are measured using a Texas Instruments quartz spiral low-pressure gage which is precise to ±0.15 kPa.

The responses of both DME and R22 were not adequately fit using the linear relationship given by eq 1. Instead, a second-order polynomial

$$n_i = k_{1i} A_i + k_{2i} A_i^2 \tag{2}$$

was used to fit the calibration data to within the accuracy of the pressure gage. The overall accuracy of composition measurement in mole fraction, including sampling and analysis errors, is estimated to be ±0.002.

Materials. The dimethyl ether was obtained from Ideal Gas Products at a claimed purity of 99.0%. It was further purified using a low-temperature distillation apparatus to an estimated purity (using gas chromatography) of at least 99.9%. The chlorodifluoromethane was obtained from Matheson Gas Products at a reported purity of 99.9%.

Results and Discussion

The vapor–liquid equilibria for the R22 + DME mixture were measured along six isotherms from room temperature to the critical region. The mixture forms a negative (maximum boiling) azeotrope which persists to the critical line. The experimental

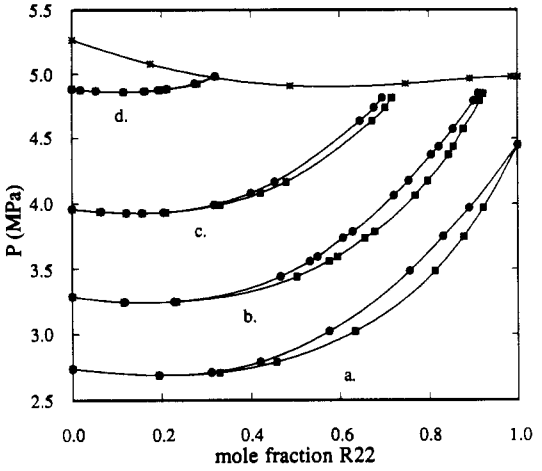

Figure 4. High-pressure $p-T-x-y$ results for R22 + DME. The isotherms are denoted by letters as follows: a, 363.15 K; b, 373.01 K; c, 383.00 K; d, 395.00 K. Experimental liquid compositions are denoted by ●. Experimental vapor compositions are denoted by ■. Experimentally observed critical points are denoted by ✱. Lines are smooth curves through the data.

Table I. $p-T-x-y$ Results for R22 (1) + DME (2)

P, MPa	x_1	y_1	P, MPa	x_1	y_1
		283.15 K			
0.374	0.0	0.0	0.363	0.505	0.595
0.350	0.163	0.130	0.382	0.557	0.672
0.341	0.252	0.235	0.415	0.625	0.763
0.338	0.331	0.333	0.469	0.712	0.852
0.338	0.357	0.368	0.531	0.798	0.921
0.348	0.439	0.493	0.681	1.0	1.0
		323.15 K			
1.149	0.0	0.0	1.173	0.482	0.550
1.108	0.133	0.120	1.224	0.547	0.632
1.098	0.231	0.227	1.323	0.636	0.740
1.098	0.271	0.273	1.501	0.757	0.856
1.102	0.314	0.326	1.752	0.895	0.951
1.112	0.360	0.387	1.947	1.0	1.0
1.139	0.427	0.474			
		363.15 K			
2.738	0.0	0.0	3.483	0.757	0.814
2.690	0.195	0.193	3.747	0.832	0.878
2.711	0.311	0.330	3.967	0.891	0.922
2.791	0.421	0.456	4.451	1.0	1.0
3.023	0.576	0.634			
		373.01 K			
3.284	0.0	0.0	4.062	0.722	0.769
3.244	0.118	0.115	4.175	0.755	0.798
3.249	0.228	0.233	4.374	0.806	0.844
3.441	0.466	0.504	4.437	0.823	0.856
3.559	0.533	0.576	4.572	0.855	0.878
3.593	0.550	0.595	4.790	0.901	0.916
3.735	0.608	0.656	4.847	0.912	0.923
3.784	0.630	0.679			
		383.00 K			
3.957	0.0	0.0	4.081	0.400	0.421
3.936	0.065	0.057	4.166	0.454	0.479
3.928	0.122	0.121	4.632	0.646	0.673
3.926	0.157	0.157	4.735	0.678	0.703
3.932	0.205	0.210	4.813	0.696	0.717
3.991	0.318	0.332			
		395.00 K			
4.882	0.0	0.0	4.873	0.194	0.197
4.873	0.020	0.019	4.881	0.212	0.213
4.865	0.054	0.054	4.923	0.276	0.281
4.858	0.116	0.115	4.979	0.321	0.321
4.864	0.162	0.164			

results are shown in Figures 2–4 and tabulated in Table I. The curves through the two lower temperature isotherms in Figures 2 and 3 are calculated using the excess Gibbs free energy model described below. The curves through the four higher temperature isotherms in Figure 4 are spline fits.

Table II. Extrapolated Azeotropic Pressure and Composition for R22 (1) + DME (2)

T, K	p_{az}, MPa	$x_{1,az}$	T, K	p_{az}, MPa	$x_{1,az}$
283.15	0.338	0.32	373.01	3.241	0.16
323.15	1.098	0.26	383.00	3.926	0.15
363.15	2.691	0.21	395.00	4.858	0.11

Table III. Results of Fitting Excess Gibbs Free Energy Model to Data for R22 (1) + DME (2)

T, K	rms Δp, MPa	rms ΔT, K	rms Δx	rms Δy	B_{12}, cm^3/mol
283.15	0.001	0.001	0.0013	0.0011	−1500
323.15	0.002	0.008	0.0006	0.0016	−600

Model Constants

$A_{00} = 3.023$ $A_{01} = -1309.62$
$A_{10} = 0.710$ $A_{11} = -259.07$
$A_{20} = -0.341$ $A_{21} = 128.27$

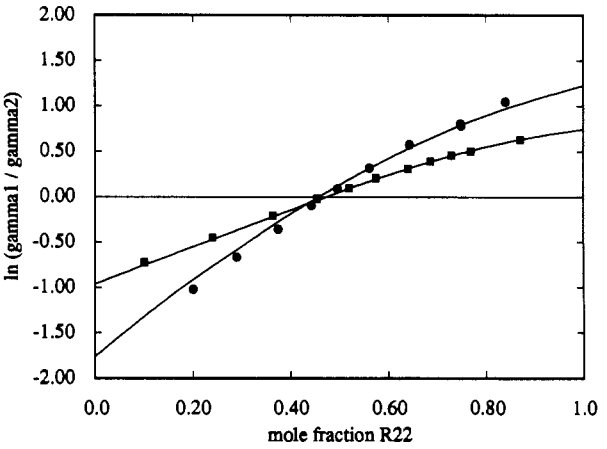

Figure 5. Equal area test for R22 + DME. The 283.15 K data are denoted by ■. The 323.15 K data are denoted by ●. The lines are excess Gibbs free energy model prediction.

The azeotropic composition, x_{az}, and azeotropic pressure, p_{az}, are estimated for each isotherm by interpolation using p versus $x - y$ plots and p versus x plots, respectively, and are listed in Table II. The azeotropic composition interpolation is sensitive to small errors in composition measurement. Therefore, the uncertainty in x_{az} is fairly high (±0.02). The uncertainty in p_{az} is no more than the measurement uncertainty (±0.003 MPa) because the isotherms are horizontal at the azeotrope.

The two lower temperature isotherms were fitted to a temperature-dependent Redlich–Kister excess Gibbs free energy model

$$G^E/RT = x_1x_2[A_{00} + A_{01}/T + (A_{10} + A_{11}/T) \times (x_1 - x_2) + (A_{20} + A_{21}/T)(x_1 - x_2)^2 \quad (3)$$

using a maximum likelihood method (*13*). The vapor phase is modeled using a virial series truncated after the second coefficient. The virial coefficients used for pure DME are those of Osipiuk and Stryjek (*15*). The virial coefficients used for pure R22 are obtained from a correlation of the data of five researchers (*11*). The cross second virial coefficients are not available for this system; therefore, the cross coefficients are chosen at each temperature to give the best overall fit to the data. In order to implement the maximum likelihood method, an accurate vapor pressure equation is needed to adjust the vapor pressures due to uncertainties in the temperature measurement. For this purpose, a three-parameter vapor pressure equation developed by Iglesias-Silva et al. (*16*) is used. The

Table IV. Critical Line for R22 (1) + DME (2)

T, K	p, MPa	x_1	T, K	p, MPa	x_1
369.00	4.976	1.0	391.47	4.908	0.489
369.97	4.976	0.985	397.28	5.076	0.176
375.78	4.963	0.893	399.40	5.264	0.0
382.62	4.922	0.748			

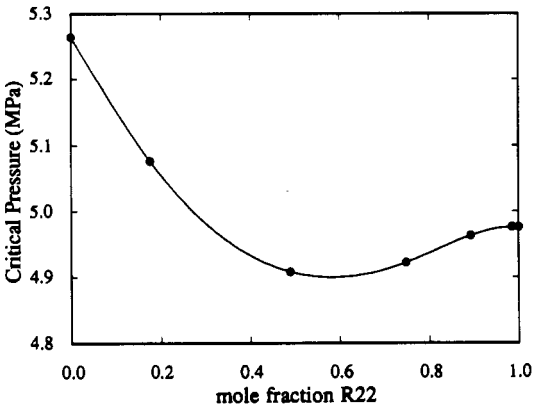

Figure 6. Composition dependence of the critical pressure for R22 + DME. Experimentally observed critical points are denoted by ●. The line is a smooth curve through the data.

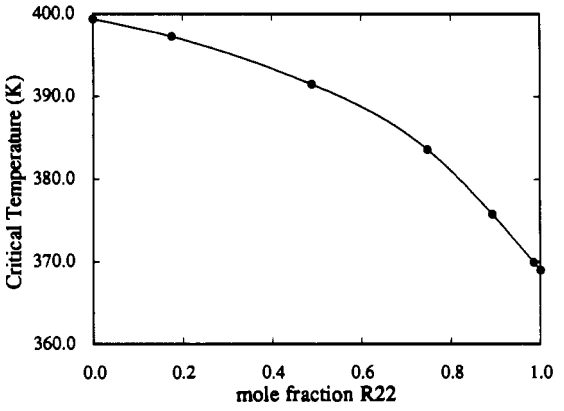

Figure 7. Composition dependence of the critical temperature for R22 + DME. Experimentally observed critical points are denoted by ●. The line is a smooth curve through the data.

results of the maximum likelihood fit are tabulated in Table III and shown in Figures 2 and 3.

The thermodynamic consistency was investigated using an equal area test (*17*). The results are shown in Figure 5. The curves are calculated using the model constants given in Table III. Quantifying the equality of areas from the data is difficult since there are no data in the dilute composition ranges. Since the curves are constrained to be thermodynamically consistent, the lack of systematic deviations from the curves is a measure of consistency.

The critical line was determined by direct observation. The temperature, of mixtures of different overall composition and approximately at the critical density, is slowly increased until the gas–liquid miniscus disappears and critical opalesence is observed. The mixture is taken through the critical point several times by lowering and raising the temperature. Once the critical pressure and temperature are determined, the mixture is taken to approximately 5 °C above the critical temperature, to insure uniformity of phase and composition, and a sample is taken and analyzed. The results of this procedure are given in Table IV. The critical loci are shown in Figures 6 and 7.

The pressure–temperature projection of the azeotropic pressures along with the pure component vapor pressure curves and the critical line is shown in Figure 8. The azeotropic vapor pressure curve intersects the critical line tangentially.

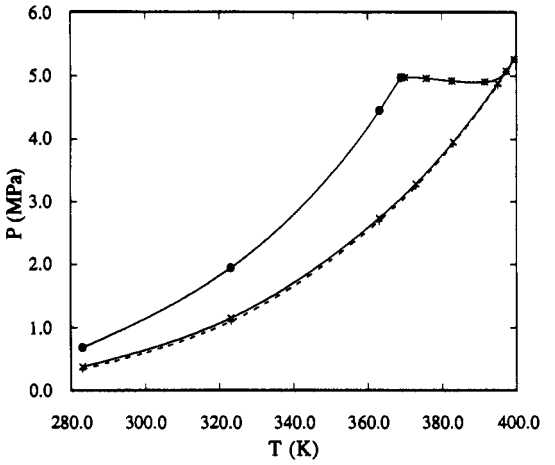

Figure 8. Pressure–temperature projection for R22 + DME. Experimental DME vapor pressure measurements are denoted by ×. Experimental R22 vapor pressure measurements are denoted by ●. Experimental critical point measurements are denoted by ✳. Extrapolated azeotropic points are denoted by +. Solid lines are smooth curves through the pure component vapor pressure points. The dashed line is a smooth curve through the azeotropic points.

Conclusions

The vapor–liquid equilibria ($p-T-x-y$) of chlorodifluoromethane + dimethyl ether have been measured for the first time along six isotherms. The mixture exhibits absolute negative (maximum boiling) azeotropy. The two lower temperature isotherms are shown to be thermodynamically consistent within experimental error. The composition dependencies of the critical pressure and temperature have been measured.

List of Symbols

A_i	integrated peak area from thermal conductivity detector
A_{mn}	constants in Redlich–Kister expansion of excess Gibbs free energy
B_{12}	cross second virial coefficient
G^E	molar excess Gibbs free energy
k_i	linear thermal conductivity response factor for component i
k_{1i}, k_{2i}	nonlinear thermal conductivity response factor constants for component i
n_i	moles of component i
p	pressure
p_{az}	azeotropic pressure
R	gas constant
T	temperature
x, x_i	liquid phase mole fraction
x_{az}	azeotropic mole fraction
y, y_i	vapor phase mole fraction

Registry No. R22, 75-45-6; DME, 115-10-6.

Literature Cited

(1) Chang, C. D.; Silvestri, A. J. *J. Catal.* **1977**, *47*, 249.
(2) Walsh, J. M.; Ikonomou, G. D.; Donohue, M. D. *Fluid Phase Equilib.* **1987**, *33*, 295.
(3) Pennington, W. A.; Reed, W. H. *Mod. Refrig.* **1950**, *May 18*, 123.
(4) Morrison, G.; McLinden, M. O. NBS Technical Note 1226, 1986.
(5) Chapman, W. G.; Gubbins, K. E.; Joslin, C. G.; Gray, C. G. *Fluid Phase Equilib.* **1986**, *29*, 337.
(6) Ikonomou, G. D.; Donohue, M. D. *AIChE J.* **1986**, *32*, 1716.
(7) Winkelmann, J. *Fluid Phase Equilib.* **1983**, *11*, 207.
(8) Keunen, J. P. *Z. Phys. Chem.* **1901**, *37*, 485.
(9) Swietoslawski, W.; Kregiewski, A. *Bull. Acad. Pol. Sci., Ser. Sci. Chim.* **1954**, *2*, 77.
(10) Khazanova, N. E.; Sominskaya, E. E.; Zakharova, A. V. *Russ. J. Phys. Chem.* **1977**, *51*, 1610.
(11) Noles, J. R. Ph.D. Dissertation, Cornell University, Ithaca, NY, 1991.

(12) Noles, J. R.; Zollweg, J. A. *Fluid Phase Equilib.* **1991**, *66*, 275.
(13) Bridgman, P. W. *The Physics of High Pressure*; G. Bell and Sons: London, 1958; p 32.
(14) Zollweg, J. A. *Thermodynamics of the Liquid Mixture Krypton + Xenon up to 190 K*; GRI Publication 91-0089; Chicago, March, 1991.
(15) Osipiuk, B.; Stryjek, R. *Bull. Acad. Pol. Sci., Ser. Sci. Chim.* **1970**, *18*, 289.
(16) Iglesias-Silva, G. A.; Holste, J. C.; Eubank, P. T.; Marsh, K. N.; Hall, K. R. *AIChE J.* **1987**, *33*, 1550.
(17) Prausnitz, J. M. *Molecular Thermodynamics of Fluid-Phase Equilibria*; Prentice-Hall: Englewood Cliffs, NJ, 1969.

Received for review September 9, 1991. Accepted February 21, 1992.

Use of Mixing Rules in Predicting Refractive Indices and Specific Refractivities for Some Binary Liquid Mixtures

Aleksandar Ž. Tasić,* Bojan D. Djordjević, and Dušan K. Grozdanić

Faculty of Technology and Metallurgy, University of Belgrade, 11000 Beograd, Karnegieva 4, Yugoslavia

Nenad Radojković

Faculty of Mechanical Engineering, University of Niš, 18000 Niš, Yugoslavia

Refractive indices for the systems benzene–cyclohexane, acetone–benzene, and acetone–cyclohexane have been measured at 25 °C over the composition range. These results, combined with the corresponding densities published earlier by us, were used to test the applicability of the Lorentz–Lorenz, Gladstone–Dale, Wiener, Heller, and Arago–Biot refractive index mixing rules. The Lorentz–Lorenz relation gave the best correlation for all systems investigated. The specific refractivities for mixtures studied were also calculated.

Introduction

Experimental data of physical properties such as refractive index are required for a full understanding of the thermodynamic properties of liquid mixtures, as well as for practical chemical engineering work. Some of the important investigations, which contributed to the development of the treatment of refractive index for liquid mixtures, have been given in refs 1–3. In order to correlate the refractive index for a binary solution of a specified composition, the mixing rules of Lorentz–Lorenz, Gladstone–Dale, Wiener, Heller, and Arago–Biot are most frequently employed. Some of these relations are not suitable when there is a large change of volume on mixing, resulting from physical and/or chemical interactions. Since the constituents of the binary systems studied are of a different nature (cycloparaffin, aromatic, and ketone), their behavior in a particular mixture will be specific and depends on its composition.

In the present work the applicability of the mixing rules to calculate the refractive index data for the binary mixtures benzene–cyclohexane, acetone–benzene, and acetone–cyclohexane at 25 °C was examined.

Experimental Section

Chemicals. Analytical grade acetone, supplied by Merck, was dried over anhydrous calcium chloride (Merck) and fractionated before use. "Analar" benzene from BDH was shaken with concentrated sulfuric acid until the yellow color in the acid layer disappeared, washed with water, and dried with sodium. Finally, it was distilled twice. Only the middle cuts were used for experimental work. "RP" cyclohexane from Carlo Erba was stirred with a mixture of HNO_3 and H_2SO_4 to remove benzene, washed with NaOH solution and water, dried with sodium, and fractionated.

Table I. Comparison of Refractive Indices n_D and Densities ρ of Pure Compounds with the Selected Literature Data at 25 °C

	n_D[a]		ρ/(g cm^{-3})	
compound	exptl	lit.	exptl	lit.
acetone	1.3557	1.355 99 (*4*) 1.356 09	0.785 08	0.785 01 (*4*) 0.785 07 0.785 08
benzene	1.4978	1.497 92 (*5*)	0.873 60	0.873 6 (*5a*)
cyclohexane	1.4231	1.423 54 (*5*)	0.773 86	0.773 89 (*5b*)

[a] Data apply to the sodium D-line.

Physical properties of the purified chemicals are given and compared with the selected literature data in Table I.

Measurements. Mixtures of the desired composition were prepared by weight using a Mettler H20 balance. The accuracy of the balance was 0.1 mg. The mixing cell and the procedure for preparing mixtures from liquids having different volatilities have been described previously (*6*). Refractive indices of the mixtures at the sodium D-line were measured with a Carl Zeiss Abbe refractometer, thermostated at 25 ± 0.010 °C. The precision of the measurements was ±0.0001 refractive index units.

Densities of the pure compounds and of their mixtures were measured previously (*6*, *7*) using an oscillator-type densimeter (DMA 02C Anton Paar) (*8*).

Mixing Rules. Since the mixtures are composed of constituents belonging to different classes of compounds, various molecular interactions are present. In that sense, the applicability of the most important mixing rules (suitable for predicting refractive indices in various physical situations) to the binaries under consideration has been tested.

The following mixing rules were used: the Lorentz–Lorenz equation (*9*)

$$\frac{n_{12}^2 - 1}{n_{12}^2 + 2} = \phi_1\left(\frac{n_1^2 - 1}{n_1^2 + 2}\right) + \phi_2\left(\frac{n_2^2 - 1}{n_2^2 + 2}\right) \quad (1)$$

where $\phi_i = w_i\rho_{12}/\rho_i$, $w_i = m_i/(m_1 + m_2)$, and $i = 1$ and 2, or in terms of specific refractivity

$$\left(\frac{n_{12}^2 - 1}{n_{12}^2 + 2}\right)\frac{1}{\rho_{12}} = \left(\frac{n_1^2 - 1}{n_1^2 + 2}\right)\frac{w_1}{\rho_1} + \left(\frac{n_2^2 - 1}{n_2^2 + 2}\right)\frac{w_2}{\rho_2} \quad (2)$$

the Wiener relation (*10*)

0021-9568/92/1737-0310$03.00/0